Photonics-Based Radar-Lidar Integrated System for Multi-Sensor Fusion Applications

Zhongyang Xu, Jianing Zhao, Fangzheng Zhang, *Senior Member, IEEE*, Lejing Zhang, Tianwen Yang, Qinru Li, and Shilong Pan, *Senior Member, IEEE*

Abstract—**A photonics-based radar-lidar integrated system is proposed, which consists of a photonics-based radar and a frequency-modulated continuous-wave (FMCW) lidar. Since the photonic generation of RF signals is used, the transmitter can simultaneously generate linear frequency-modulated (LFM) radio-frequency (RF) and optical signals. Meanwhile, similar data acquisition methods are shared by the radar and lidar subsystems because FMCW ranging method is used in both of them. In the integrated system, the lidar subsystem provides high-resolution 3D images and velocity distributions, while the radar subsystem can implement real-time imaging with high frame rates. An experiment is carried out, in which a system consisting of a K-band radar and a 1550-nm FMCW lidar is used. The bandwidth of the radar and lidar subsystems are 8-GHz and 4-GHz. The standard deviations of displacements between the measured and the expected distances are 0.342 cm and 0.997 cm for the radar and lidar subsystems, respectively. For multi-sensor fusion applications, the 3D image and velocity distribution of a static cardboard and a spinning disk are obtained by the lidar subsystem, while the inverse synthetic aperture (ISAR) imaging for the spinning disk is achieved by the radar subsystem. Since some parts of the system are shared by the lidar and radar subsystems, the integrated system has a compact configuration, which is a potential configuration of the on-chip radar-lidar fusion system. Moreover, the performance of the lidar and radar subsystems are higher than the commonly used radar-lidar fusion system, which can be further enhanced by sophisticated data fusion algorithms.**

Index Terms—**Photonics-based radar, frequency-modulated continuous-wave lidar, multi-sensor fusion.**
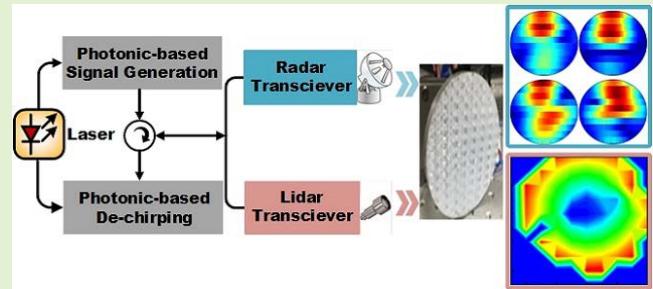
I. INTRODUCTION

BOTH of radars and lidars are the widely used active sensors that extract the information of targets from the backscattered signals [1]–[5]. The difference between them is that radars use radio-frequency (RF) signals, while lidars transmit optical signals. In many applications, both of the information in the RF and optical regime are required to achieve an overall perception of targets. As a result, a multi-sensor fusion system consisting of lidars and radars are highly demanded to extract multi-domain information [6]–[8]. Moreover, as a multi-sensor system, a radar-lidar fusion system has good applicability and performance. For example, the lidars are invulnerable to RF interference, and the radars are robust

against the adverse weather. Using a fusion system, both of the advantages of lidars and radars can be employed so that the system can work with low errors in complex environments [9]–[11]. Due to these features, radar-lidar fusion systems have been used in automotive driving and remote sensing. The fusion of lidars and radars in automotive driving can detect partially obscured objects, enable sufficient coverage for long and short-range applications, and increase the confidence of detection [6], [7], [9].

However, in those systems, separate lidar and radar systems work independently and only the data fusion is adopted. To meet the cost and space restrictions in multi-sensor applications, integrated systems are highly demanded. But, nowadays, there are still challenges to integrate lidars and radars into a compact system. Firstly, in a radar system, RF signals are usually generated via fully electronic techniques while the optical signals have to be generated in the lidar subsystem. Secondly, different data acquisition methods are required for the subsystems because an FMCW radar [12] and a time-of-flight lidar [13] are respectively used in common radar-lidar fusion applications [14].

Recently, photonics-based radar systems with frequency flexibility and high performance have been proposed [15]–[18]. Using the photonic generation of RF signals, a radar

can operate at multiple bands [16] with high-frequency carriers and large bandwidths [18]. Meanwhile, real-time radar imaging can be achieved due to the use of photonics-based detection of RF signals [17]–[19]. The use of photonic techniques not only improves the performance of radars but also provides a promising approach for radar-lidar integrated systems, since the optical and RF signals can be simultaneously generated in the transmitter. For example, in [20] and [21], a radar-lidar integrated system is built based on a mode-locked laser. The multiple tones of the mode-locked laser are used for a Doppler lidar, while the beat signals of the tones are used to generate RF signals for a radar. This radar-lidar integrated system can be used for multi-sensor applications [22], in which the velocity is obtained by the lidar subsystem and SAR imaging is achieved by the radar system. However, the spatial resolution of the system is not sufficient good, since the bandwidth is small and laser beam-steering is not used. Besides, the mode-lock laser used in the system is complex and highly-cost.

A photonics-based radar system can also be achieved by photonic frequency multiplication using electro-optical modulators [17]–[19]. The radar has a larger bandwidth than that in [15] and [16]. Moreover, in the systems, linear frequency-modulated (LFM) optical and RF signals are simultaneously generated in the transmitter, Among which, the LFM RF signal is used in a radar system, while the LFM optical signal can be used for a frequency-modulated continuous-wave (FMCW) lidar to implement simultaneous ranging and velocimetry [23], [24]. In addition, since FMCW ranging method [25], [26] are used in the radar and the FMCW lidar systems, similar signal processing methods can be shared by them so that the data acquisition module in a radar-lidar integrated system can be shared by the radar and lidar subsystems. As far as we know, such a radar-lidar integrated system has not been reported.

In this work, we propose a radar-lidar integrated system consisting of a photonics-based radar and an FMCW lidar. In the transmitter, a carrier-suppressed dual-sideband (CS-DSB) optical signal is generated at a dual-parallel Mach-Zehnder modulator (DP-MZM). One part of the light is directly used as the lidar signal, while the radar signal is generated from the beat signal between the two optical sidebands of the CS-DSB optical signal. In the receiver, the local optical (LO) signal is also a CS-DSB optical signal. The reflected light beats with the LO signal to obtain a de-chirped lidar signal. Meanwhile, the echo radar signal is processed by the photonic-assisted de-chirping to obtain a de-chirped radar signal. An experiment is carried out, in which a K-band photonics-based radar with a bandwidth of 8 GHz and a 1550-nm FMCW lidar with a bandwidth of 4 GHz are integrated into a system. The performance of the radar and lidar subsystems are evaluated and the multi-sensor applications are demonstrated, in which a static cardboard with a complex profile and a spinning disk are respectively used as the target. 3D images and velocity distribution of the targets are obtained by the lidar system. Meanwhile, high-frame-rates ISAR imaging for the moving targets can be achieved via the radar subsystem. Comparing with the previous radar-lidar fusion system, the integrated system has a compact configuration, which is a promising
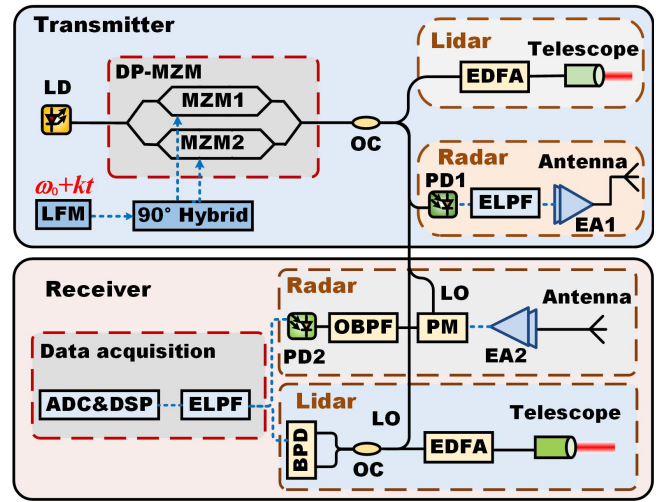

Fig. 1. Schematic diagram of the proposed radar-lidar integrated system. LD: laser diode; DP-MZM: dual-parallel Mach-Zehnder modulator, LFM: linear frequency-modulated signal. OC: optical coupler, EDFA: Erbium-doped fiber amplifier, PD: photodetector, EA: electrical amplifier, PM: phase modulator, LO: local optical signal, OBPF: optical band-pass filter, BPD: balanced photodetector, ELPF: electrical low pass filter.

configuration for an on-chip radar-lidar integrated system. Moreover, the performance of the lidar and radar subsystems are higher than the commonly used radar-lidar fusion system, which promises a robust multi-sensor fusion system with small size, high-resolution, and high-frame-rates.

II. SYSTEM AND PRINCIPLE

Figure 1 shows the schematic diagram of the proposed radar-lidar integrated system. The solid black lines represent optical fibers. The blue dashed lines are electrical cables. In the transmitter, a continuous lightwave is modulated at a DP-MZM. An LFM signal is generated by a low-speed electrical signal generator, which is split by a 90-degree hybrid and used to drive the two sub-MZMs of the DP-MZM (i.e., MZM1 and MZM2), respectively. By biasing the two sub-MZMs at the maximum transmission point, the output signals of the two sub-MZMs can be expressed as

$$
\begin{aligned}
E_1 &= A_1 \cos\left\{\beta \cos\left[(\omega_0 + kt)\, t\right]\right\} e^{i\omega_c t} \\
E_2 &= A_2 \cos\left\{\beta \cos\left[(\omega_0 + kt)\, t + \frac{\pi}{2}\right]\right\} e^{i\omega_c t}
\end{aligned} \tag{1}
$$

where A_1 and A_2 are the magnitudes of the output signals of MZM1 and MZM2, $\omega = \omega_0 + 2kt$ is the instantaneous angular frequency of the LFM signal. β and ω_c are the modulation index and the angular frequency of the optical carrier. The optical phase difference between the two sub-MZMs is set to π so that the output signal of the DP-MZM can be expressed as

$$
\begin{aligned}
E_{\text{DP-MZM}} &= A_1 \cos\left\{\beta \cos\left[(\omega_0 + kt)\, t\right]\right\} e^{i\omega_c t} \\
&+ A_2 \cos\left\{\beta \cos\left[(\omega_0 + kt)\, t + \frac{\pi}{2}\right]\right\} e^{i(\omega_c t + \pi)}
\end{aligned} \tag{2}
$$

Using Jacobi-Anger expansion, (2) can be expanded as

$$
\begin{aligned}
E_{\text{DP-MZM}} &\propto J_2(\beta) \cos\left[\omega_c t + 2(\omega_0 + kt)\, t\right] \\
&+ J_2(\beta) \cos\left[\omega_c t - 2(\omega_0 + kt)\, t\right]
\end{aligned} \tag{3}
$$

where $J_2(\beta)$ is the 2nd-order Bessel function of the first kind. Then, the modulated light is split into four parts by an optical coupler. The first part is used as the transmitted signal of the lidar subsystem. The second part is converted to the transmitted signal of the radar subsystem by a photodetector, which can be expressed as

$$E_{\text{Radar}} \propto [J_2(\beta)]^2 \cos[4(\omega_0 + kt)t] \quad (4)$$

The other two parts of the light are used as the LO signals of the radar and lidar subsystems, respectively. It should be noted that the radar signal in (4) is frequency quadrupled to obtain a high-frequency RF carrier and a large bandwidth.

In the receiver, the reflected optical signal in the lidar subsystem is collected and beats with the LO lidar signal in a balanced photodetector (BPD) to generate a de-chirped lidar signal, which is given by

$$I_{\text{lidar}} \propto J_2(\beta)\cos(4k\tau t + \omega_d t) + J_2(\beta)\cos(4k\tau t - \omega_d t) \quad (5)$$

where ω_d is the optical Doppler frequency shift (DFS), $\tau = 2R/c$ is the time delay of the reflected optical signal. R and c are the distance of the target and the speed of light in vacuum. It should be noted that the lidar subsystem is a CS-DSB FMCW lidar so that a dual-frequency de-chirped signal can be obtained. The sum and the difference of the two frequencies can be respectively used to calculate the distance and velocity [23].

For the radar subsystem, the RF echo is processed by photonic-assisted de-chirping in the receiver [17], [18]. The echo RF signal is firstly used to drive a phase modulator, in which the LO optical signal is modulated. Then, the LO signal is detected by a photodetector to generate a de-chirped radar signal, which can be written as

$$I_{\text{radar}} \propto \cos(8k\tau t) \quad (6)$$

Since the bandwidth of the LFM signal in (4) is enlarged 4 times, the distance resolution of the photonics-based radar is enhanced by 4 times. According to (5) and (6), similar signal processing methods can be used for the lidar and radar subsystems. In the data acquisition module, an electrical low pass filter (ELPF) is first used to obtain the de-chirped lidar signals and radar signals. Then, an analog-to-digital converter (ADC) is used to convert the signals into digital signals. The short-time Fourier transform is used to extract the spectra of the digital signals. Finally, the peak frequencies in the spectra are used to calculate the distances and velocities, in which wideband receivers can be avoided [27].

III. EXPERIMENT AND DISCUSSION

An experiment is carried out, in which the performance of the radar-lidar integrated system is evaluated. In the system, a 1550-nm lightwave from a narrow linewidth laser diode (TeraXion Inc.) is modulated at a DP-MZM (Fujitsu FTM7962EP). A 4.5-6.5 GHz LFM RF signal with a period of 50 μs is used to drive the DP-MZM. A CS-DSB optical signal with only the $\pm$2nd-order sidebands is generated. The power of the LO signal is around 2 mW and the transmitted optical signal is around 200 mW. The light beam is collimated and the spot
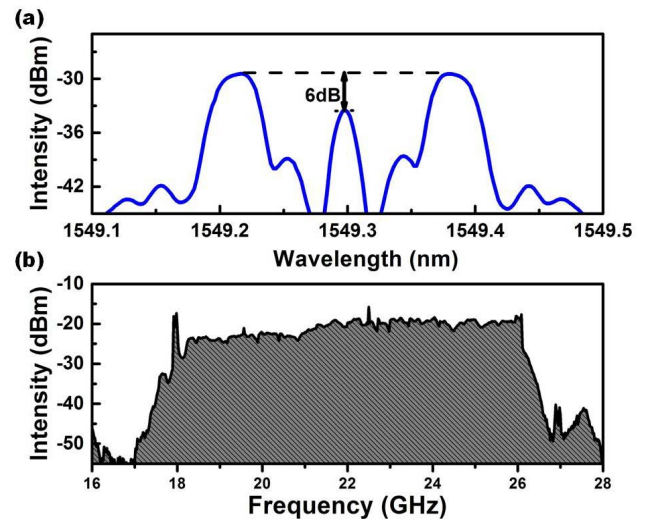

Fig. 2. (a) Optical spectrum of the transmitted lidar signal. Only the $\pm$2nd-order sidebands are generated with 6-dB carrier-suppression ratio. (b) Spectrum of the transmitted radar signal. An 18-26 GHZ broadband signal is generated for radar subsystem.

diameter is around 10 mm. Fig.2 shows the optical spectrum of the transmitted lidar signal and the spectrum of the transmitted radar signal. For the FMCW lidar subsystem, the frequency shifts of the $\pm$2nd-order optical sidebands are $\pm$ (9-13) GHz so that the bandwidth of the lidar is 4 GHz. The two sidebands have opposite chirp rates and the carrier-sideband intensity ratio is around 6 dB. For the photonics-based radar subsystem, an electrical band-pass filter is used to select the beat signal between the $\pm$2nd-order sidebands so that an 18-26 GHz RF signal is generated. The bandwidth of the transmitted radar signal is 8 GHz and the out-of-band rejection is more than 20 dB. In the receiver, a BPD (Thorlabs PDB450C) with a bandwidth of 150 MHz is used to obtain the de-chirped lidar signal. The same devices as that used in the previous work [9] are used to get the de-chirped radar signal via photonic-assisted de-chirping. Finally, the de-chirped lidar and radar signals are recorded and processed to extract the information of targets

A photograph of the prototype of the radar-lidar integrated system is shown as Fig. 3(c). The signal generation module and the signal processing module are included in the black box. The radar signal is transmitted by the antenna in the front of the box, while one part of the optical signal in the black box is extracted and amplified by an EDFA. The amplified optical signal is used as the lidar signal and transmitted by a telescope on a rotatable platform. The size of the system is comparable to the radar-lidar fusion system in [14]. But, since it is a prototype, the size of the proposed system can be further miniaturized with small beam-scanning devices. To evaluate the performance of the radar and lidar subsystems, the distance resolutions of the radar and lidar subsystems are measured. In the experiment, the signal backscattered from the target is recorded using a real-time oscillator and off-line processed. Two closed corner reflectors and a movable mirror are respectively used as the targets for the radar and lidar subsystems. The two corner reflectors are spaced by
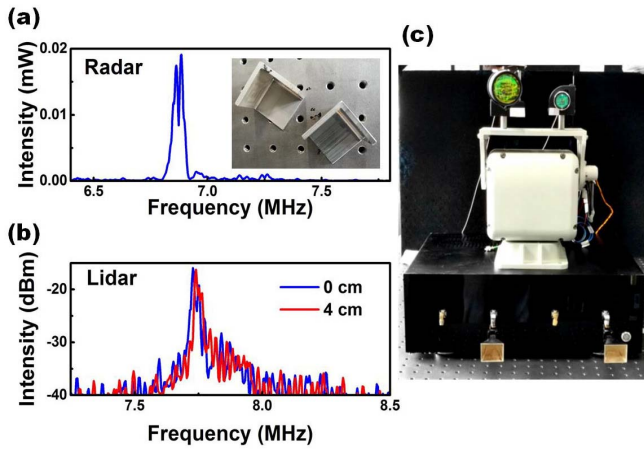
Fig. 3. (a)-(b) Ranging resolution of the radar and the lidar subsystems. (a) The spectrum of the de-chirped radar signal reflected by two corner reflectors. (b) The spectra of the de-chirped lidar signal reflected by a mirror at different positons. (c) The appearance of the lidar-radar integrated system.
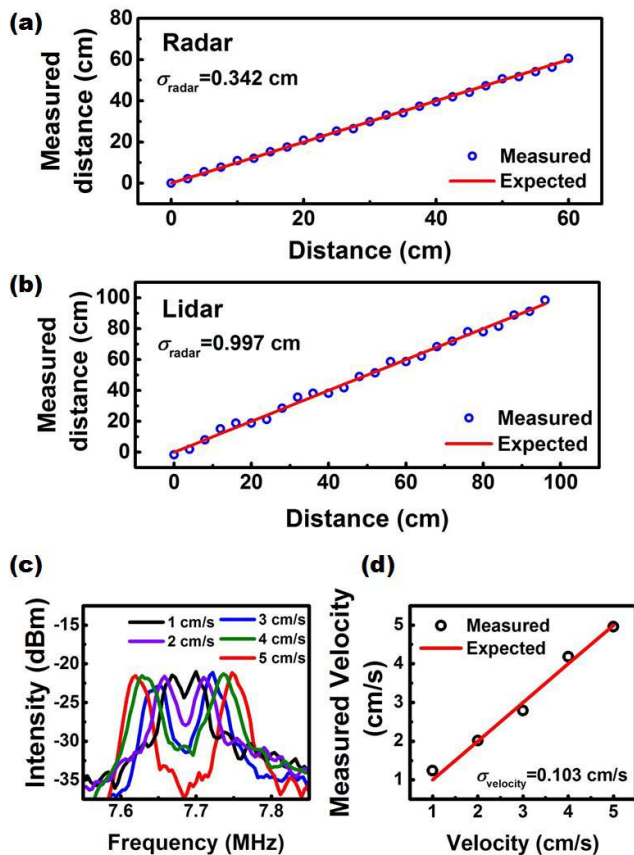

Fig. 4. Performance of the radar and lidar subsystems. (a)-(b) The ranging performance of the radar and lidar subsystems, respectively. (c)-(d) The velocimetry performance of the lidar subsystem.
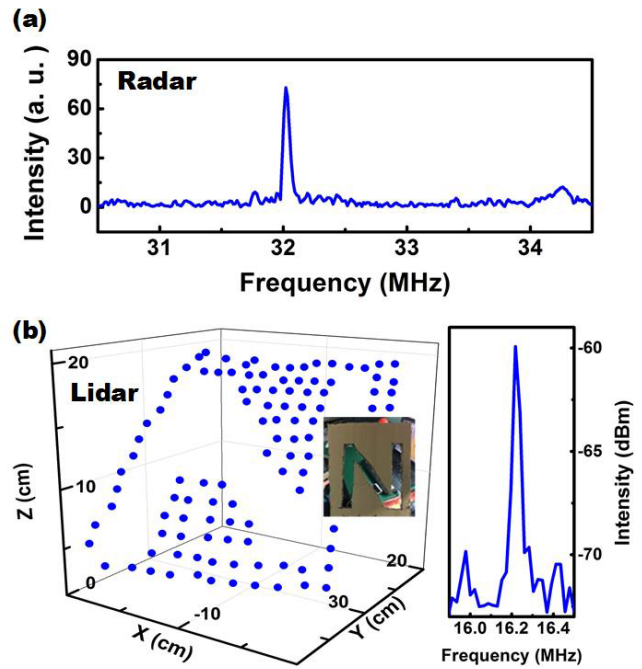

Fig. 5. Measurements of a static cardboard. (a) The spectrum of the de-chirped radar signal. (b) Left: the 3D image measured by the lidar. Inset: the photograph of the cardboard. Right: the spectrum of the de-chirped lidar signal at one measurement point.

2.5 cm. The spectrum of the de-chirped radar signal is shown in Fig. 3 (a), which has two separate peaks. On the other hand, the mirror is successively placed at a distance of 0 cm and 4 cm. The spectra of the de-chirped lidar signal at two different distances are shown in Fig. 3(b). According to the measurement result, the practical resolutions of the radar and lidar subsystems are around 2.5 cm and 4 cm, even

though the theoretical distance resolution of the radar and lidar is 1.875 cm and 3.75 cm, according to $\delta R = c/2B$. More measurements are implemented to estimate measurement errors. Fig. 4(a) and (b) shows the different distances measured by the radar and lidar, respectively. The standard deviations of the displacements between the measured distances and the expected values are 0.342 cm and 0.997 cm for the radar and lidar subsystems. Moreover, the performance of the lidar velocimetry is also evaluated. The spectra of the de-chirped lidar signal are shown in Fig. 3(c), in which all the spectra shows two peaks. The full width at half maximum (FWHM) of the peaks are less than 0.032MHz, which indicates a velocity resolution finer than 2.48 cm/s. Several measurements are implemented at different velocities, which are shown in Fig. 3 (d). The standard deviation of the displacements between the measured velocities and the expected values is 0.103 cm/s.

To demonstrate the applications of the proposed system in multi-sensor fusion, a cardboard with a complex profile is firstly adopted as the target. Since the RF signal has a larger angle of divergence, the radar subsystem cannot distinguish the complex profile of the cardboard. As a result, a spectrum of the de-chirped signal with a single peak is obtained by the radar subsystem in Fig. 5(a). Only the average distance of the cardboard can be extracted. The FWHM of the peak is 75 kHz, which means that the distances of the cardboard distribute in a range of 7.0 cm. For the lidar subsystem, the telescope is mounted on a 2D rotatable platform (shown as Fig. 3(c)) so that the pitch and yaw angles of the laser beam can be controlled and measured in real-time. In the experiment, one point is measured in every second and the de-chirped lidar signals at different points are recorded. One
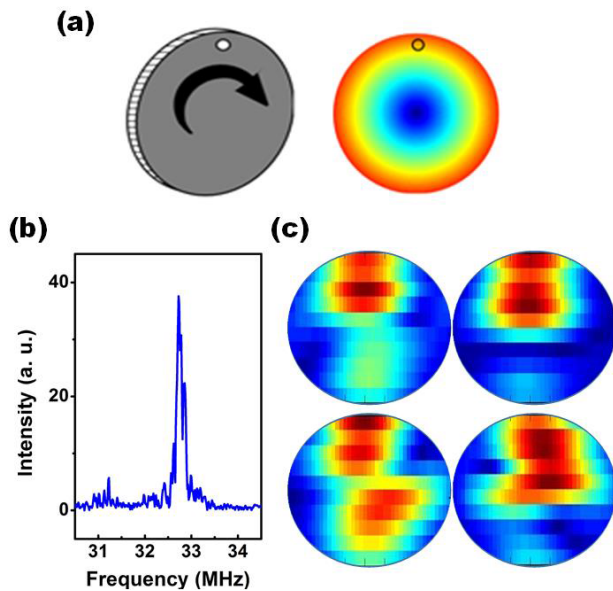
Fig. 6. Measurements of a spinning disk implemented by the radar subsystem. (a) Left: the cartoon diagram of the spinning disk. Right: the expected distribution of tangential velocities on the spinning disk. The color represents the value of tangential velocity. The small circle on the disk indicates the covered area of laser beam during a single-point measurement. (b) The spectrum of the de-chirped radar signal. (c) Four different frames of ISAR images obtained by the radar subsystem. The color represents intensity of the echoed radar signal.

of the measured spectra is shown in the right subfigure of Fig. 5 (b). The FWHM of the peak is 40 kHz, which indicates a distance resolution of 7.5 cm. The range resolution is worse than that in Fig. 3. It is because that the echo signal of the cardboard is much weaker than the mirror so that the averaged spectrum is used to suppress the noise and spur. According to the measurement results at different points, the 3D image of the cardboard is calculated and shown in the left subfigure of Fig. 5(b), in which the angular resolution is 2.5-degree. In the 3D image, only the relative distances are displayed, which clearly shows a tilted cardboard with a clear "N" on the profile. Although the lidar subsystem has a lower resolution of distance than the radar subsystem, it can achieve 3D imaging for the complex profiles of the targets due to its high angular resolution. As a result, using radar-lidar fusion, high-resolution 3D imaging may be achieved.

A spinning disk is also used to verify the capability of the proposed system to detect a moving target. The disk is shown as the cartoon diagram in the left subfigure of Fig. 6(a), which has a diameter of 10 cm and spins clockwise. The right subfigure of Fig. 6(a) shows the expected distribution of tangential velocities on the disk. For the radar subsystem, inverse synthetic aperture radar (ISAR) imaging can be implemented to detect the spinning disk. Since the photonics-based de-chirping process is employed, the photonics-based radar system can implement real-time ISAR imaging with a high frame rate as much as 100 frames per second [18]. Fig. 6(c) shows four different frames of the ISAR images of the spinning disk which are obtained by the radar subsystem. The frame rate of the ISAR imaging in the experiment is 5 frames per second and the color of the images presents the
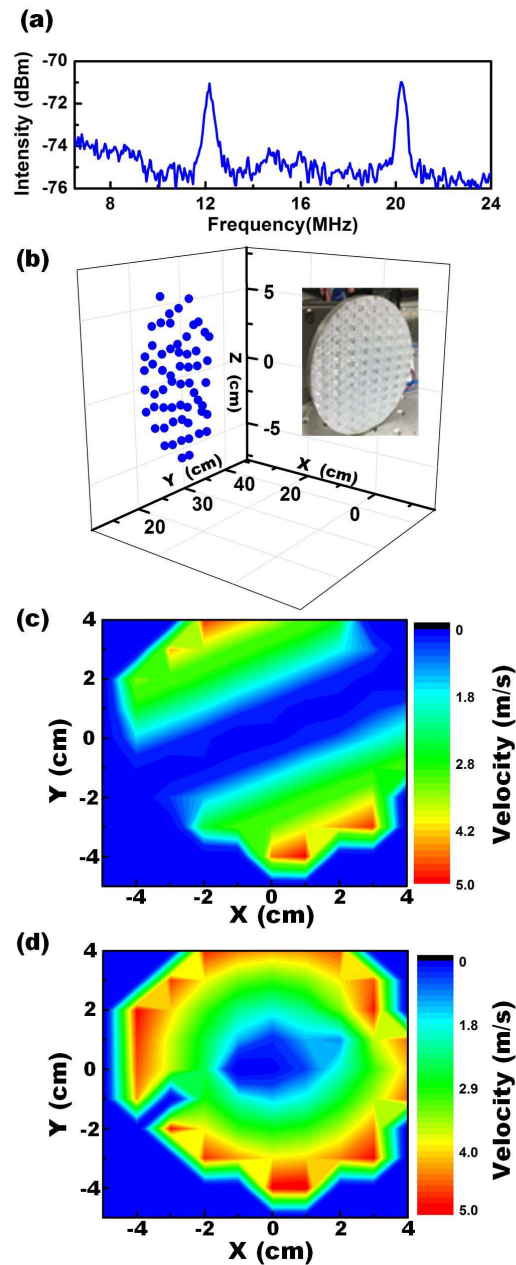

Fig. 7. Measurements of a spinning disk implemented by the lidar subsystem. (a) The spectrum of the de-chirped lidar signal, which is measured at a single point. (b) The 3D image of the spinning disk obtained by the lidar. Inset: the photograph of the disk. (c)-(d) The distribution of line-of-sight velocities and the distribution of tangential velocities on the spinning disk obtained by the lidar subsystem.

intensity of the echoed RF signal. Different profiles are shown in different frames, which indicates that the radar subsystem can sense the spin of the disk. However, the images are too blur to obtain a high-resolution image of the spinning disk. Moreover, the distribution of velocities shown in Fig. 6(a) cannot be obtained. Usually, additional techniques are required for a radar system to measure the velocity of targets in real-time [28], since DFSs of the RF signals are too small to be distinguished in the spectrum.

For the lidar subsystem, not only the distance of the spinning disk, but also the velocity information on the disk can be obtained because coherent detection is used. The measured

TABLE I
COMPARISON OF DIFFERENT RADAR-LIDAR FUSION SYSTEMS

Reference	DISTANCE ERRORS FOR RADAR	DISTANCE ERRORS FOR LIDAR	DOPPLER VELOCIMETRY	VELOCITY ERRORS FOR RADAR	VELOCITY ERRORS FOR LIDAR	INTEGRATED CONFIGURATION
[10]	0.08 m	0.094 m	No	0.301 km/h	0.795 km/h	No
[11]	0.72 m	0.26 m	No	0.48 m/s	0.29 m/s	No
[14]	0.037 m	0.011 m	No	N. A.	N. A.	No
[20-22]	>1 m	<0.1 m	Yes	<0.06m/s	<0.0063 m/s	Yes
This work	0.005 m	0.017 m	Yes	N. A.	0.00138 m/s	Yes

spectrum of the de-chirped lidar signal in the integrated system shows two peaks (Fig. 7(a)). The distance and velocity can be calculated from the sum and the difference of the two frequencies, respectively. In Fig. 7(a), the FWHM of the two peaks are much broader than that for a static target. The resulted velocity resolution is around 1.04 m/s, which is much worse than the resolution in Fig. 3(c). However, it is caused by the target rather than the system. Since the diameter of the laser spot is 10 mm, the velocities in the area covered by the beam spot (show as the black circle in Fig. 6(a)) distribute in a relatively large range. As a result, the peaks of the de-chirped lidar signal are severely broadened due to the varied DFSs, which eventually worsens the resolution of the system.

Different from the radar subsystem, the 3D image of the disk and the velocity distribution on the disk can be simultaneously obtained by the lidar subsystem. Fig. 7(b) is the 3D images of the spinning disk, in which the inset is the photograph of the disk. Fig. 7 (c) and (d) shows the measured velocity distribution on the spinning disk, in which the color presents the value of velocities. The line-of-sight velocities (Fig. 7(c)) are directly measured by the lidar subsystem, while the tangential velocities (Fig. 7(d)) are calculated according to the measured line-of-sight velocities and 3D-coordinate of the disk. The distribution of tangential velocities shows obvious annular structures, which is matched with the expected velocity distribution shown as Fig.6 (a). Since the spot size of the laser beam is 10 mm and the angular resolution is 2-degree, the spatial resolution of the velocity distribution is not very high. With better beam scanning devices, high spatial resolution images can be obtained.

Compared with the ISAR images obtained by the radar subsystem, the 3D images obtained by the lidar subsystem have lower frame rates since beam scanning is required. However, the lidar subsystem can implement high-spatial-resolution 3D imaging and velocity distribution mapping. Therefore, in a practical radar-lidar fusion system, the lidar subsystem can be used to obtain the high spatial resolution mapping of the distance and velocity, while the radar can achieve real-time imaging of the fast-changing target with high frame rates. Moreover, since photonic techniques and FMCW ranging methods are used, the measurement errors of the radar-lidar integrated system are reduced. The performances of different radar-lidar fusion systems are listed in Table I. In [10] and [11], the distance errors are more than 8 cm. Although the distance errors are reduced in [14] using SLAM algorithms, all of the three fusion systems extract velocities from the variation of the measured distances so that the velocity errors are large. Although the distance errors in [20]–[22] are

large since the bandwidth of the radar is small, the velocity errors are reduced since the coherent lidar is used so that Doppler velocimetry can be implemented. Compared with the previously reported system, the performance of our proposed radar-lidar is higher, even though data fusion algorithms are not used. The mean displacements between the measured distances and the expected values are around 0.5 cm and 1.7 cm for the radar and lidar subsystems, respectively. The mean displacement for the velocimetry is around 0.138 cm/s. With sophisticated algorithms, the performance of the system can be further enhanced.

In addition, the integrated configuration is achieved in [20]–[22] and this work because photonic techniques are used. Since FMCW lidar is suitable for the on-chip lidar system due to its low peak power [29], the integrated configuration of the proposed system promises a compact radar-lidar fusion system. Recently, the on-chip photonics-based radar for ISAR imaging has been reported [30]. The CS-DSB optical signals generated in the chip can be directly used for an FMCW lidar, which would enable an on-chip radar-lidar integrated system for multi-sensor applications.

IV. CONCLUSION

In conclusion, we propose a photonics-based radar-lidar integrated system and demonstrate its applications in multi-sensor fusion sensing. The lidar and radar subsystems partially share a transmitter in which LFM optical and RF signals are simultaneously generated. In the receiver, similar data acquisition methods are also shared by the two subsystems. The prototype of the integrated system is constructed and used to detect the static and moving targets, respectively. Since the large bandwidth and coherent detection are used, the standard deviations of the displacements for the measured distances and velocities can be reduced to 0.342 cm and 0.103 cm/s in the radar-lidar integrated system. Experiment results show that the lidar subsystem can provide the high-resolution 3D measurements for the targets since it has a high angular resolution. On the other hand, the radar subsystem has a fast frame rate since beam scanning is not needed. The radar-lidar integrated system has a compact configuration, which promises a multi-sensor fusion system with compact size and multiple functions, such as an on-chip lidar-radar fusion system.

REFERENCES

[1] B. Schwarz, "LIDAR: Mapping the world in 3D," *Nature Photon.*, vol. 4, no. 7, pp. 429–430, 2010.
[2] C. K. Toth, "Sensor integration in airborne mapping," *IEEE Trans. Instrum. Meas.*, vol. 51, no. 6, pp. 1367–1373, Dec. 2002.
[3] J. Steinbaeck, C. Steger, G. Holweg, and N. Druml, "Next generation radar sensors in automotive sensor fusion systems," in *Proc. Sensor Data Fusion, Trends, Solutions, Appl. (SDF)*, Bonn, Germany, Oct. 2017, pp. 1–6.

[4] D. Massonnet *et al.*, "The displacement field of the landers earthquake mapped by radar interferometry," *Nature*, vol. 364, no. 6433, pp. 138–142, Jul. 1993.

[5] R. C. Schnell *et al.*, "Lidar detection of leads in Arctic sea ice," *Nature*, vol. 339, no. 4, pp. 530–532, Jun. 1989.

[6] J. Hollinger, B. Kutscher, and R. Close, "Fusion of lidar and radar for detection of partially obscured objects," *Proc. SPIE*, vol. 9468, May 2015, Art. no. 946806.

[7] R. H. Rasshofer and K. Gresser, "Automotive radar and lidar systems for next generation driver assistance functions," *Adv. Radio Sci.*, vol. 3, pp. 205–209, May 2005.

[8] H. Okamoto *et al.*, "Development of a multiple-field-of-view multiple-scattering polarization lidar: Comparison with cloud radar," *Opt. Express*, vol. 24, no. 26, pp. 30053–30067, Dec. 2016.

[9] T. Herpel, C. Lauer, R. German, and J. Salzberger, "Multi-sensor data fusion in automotive applications," in *Proc. 3rd Int. Conf. Sens. Technol.*, Tainan, Taiwan, Nov. 2008, pp. 206–211.

[10] H. Lee, H. Chae, and K. Yi, "A geometric model based 2D LiDAR/radar sensor fusion for tracking surrounding vehicles," *IFAC-PapersOnLine*, vol. 52, no. 8, pp. 130–135, 2019.

[11] D. Gohring, M. Wang, M. Schnurmacher, and T. Ganjineh, "Radar/lidar sensor fusion for car-following on highways," in *Proc. 5th Int. Conf. Autom., Robot. Appl.*, Wellington, New Zealand, Dec. 2011, pp. 407–412.

[12] E. Jose, M. Adams, J. S. Mullane, and N. M. Patrikalakis, "Predicting millimeter wave radar spectra for autonomous navigation," *IEEE Sensors J.*, vol. 10, no. 5, pp. 960–971, May 2010.

[13] T. Fersch, R. Weigel, and A. Koelpin, "A CDMA modulation technique for automotive time-of-flight LiDAR systems," *IEEE Sensors J.*, vol. 17, no. 11, pp. 3507–3516, Jun. 2017.

[14] M. Mielle, M. Magnusson, and A. J. Lilienthal, "A comparative analysis of radar and lidar sensing for localization and mapping," in *Proc. Eur. Conf. Mobile Robots (ECMR)*, Prague, Czech Republic, Sep. 2019, pp. 1–6.

[15] P. Ghelfi *et al.*, "A fully photonics-based coherent radar system," *Nature*, vol. 507, no. 7492, pp. 341–345, Mar. 2014.

[16] P. Ghelfi, F. Laghezza, F. Scotti, D. Onori, and A. Bogoni, "Photonics for radars operating on multiple coherent bands," *J. Lightw. Technol.*, vol. 34, no. 2, pp. 500–507, Jan. 15, 2016.

[17] X. Ye, F. Zhang, Y. Yang, and S. Pan, "Photonics-based radar with balanced I/Q de-chirping for interference-suppressed high-resolution detection and imaging," *Photon. Res.*, vol. 7, no. 3, pp. 265–272, 2019.

[18] F. Zhang, "Photonics-based broadband radar for high-resolution and real-time inverse synthetic aperture imaging," *Opt. Express*, vol. 25, no. 14, pp. 16274–16281, Jul. 2017.

[19] F. Zhang *et al.*, "Photonics-based real-time and high-resolution ISAR imaging of non-cooperative target," *Chin. Opt. Lett.*, vol. 15, no. 11, 2017, Art. no. 112801.

[20] F. Scotti, D. Onori, M. Scaffardi, E. Lazzeri, A. Bogoni, and F. Laghezza, "Multi-frequency Lidar/radar integrated system for robust and flexible Doppler measurements," *IEEE Photon. Technol. Lett.*, vol. 27, no. 21, pp. 2268–2271, Nov. 1, 2015.

[21] V. Vercesi, D. Onori, F. Laghezza, F. Scotti, A. Bogoni, and M. Scaffardi, "Frequency-agile dual-frequency lidar for integrated coherent radar-lidar architectures," *Opt. Lett.*, vol. 40, no. 7, pp. 1358–1361, Apr. 2015.

[22] F. Scotti *et al.*, "Microwave photonics for integrated multifrequency lidar / radar system," in *Proc. Opto-Electron. Commun. Conf. (OECC)*, Shanghai, China, Jun. 2015, pp. 1–4.

[23] Z. Xu, L. Tang, H. Zhang, and S. Pan, "Simultaneous real-time ranging and velocimetry via a dual-sideband chirped lidar," *IEEE Photon. Technol. Lett.*, vol. 29, no. 24, pp. 2254–2257, Dec. 15, 2017.

[24] J. Anderson, R. Massaro, J. Curry, R. Reibel, J. Nelson, and J. Edwards, "LADAR: Frequency-modulated, continuous wave laser detection and ranging," *Photogramm. Eng. Remote Sens.*, vol. 83, no. 11, pp. 721–727, Nov. 2017.

[25] M.-C. Amann, T. Bosch, M. Lescure, R. Myllyla, and M. Rioux, "Laser ranging: A critical review of usual techniques for distance measurement," *Opt. Eng.*, vol. 40, no. 1, pp. 10–19, 2001.

[26] Y. Xiong, Z. Peng, G. Xing, W. Zhang, and G. Meng, "Accurate and robust displacement measurement for FMCW radar vibration monitoring," *IEEE Sensors J.*, vol. 18, no. 3, pp. 1131–1139, Feb. 2018.

[27] K. Hu, Y. Zhao, M. Ye, J. Gao, G. Zhao, and G. Zhou, "Design of a CMOS ROIC for InGaAs self-mixing detectors used in FM/cw LADAR," *IEEE Sensors J.*, vol. 17, no. 17, pp. 5547–5557, Sep. 2017.

[28] M. Ash, M. Ritchie, and K. Chetty, "On the application of digital moving target indication techniques to short-range FMCW radar data," *IEEE Sensors J.*, vol. 18, no. 10, pp. 4167–4175, May 2018.

[29] A. Martin *et al.*, "Photonic integrated circuit-based FMCW coherent LiDAR," *J. Lightw. Technol.*, vol. 36, no. 19, pp. 4640–4645, Oct. 1, 2018.

[30] S. Li *et al.*, "Chip-based photonic radar for high-resolution imaging," May 2019, *arXiv:1905.12802*. [Online]. Available: https://arxiv.org/abs/1905.12802

Zhongyang Xu received the B.S. degree in physics from Sun Yat-sen University, Guangzhou, China, in 2010, and the Ph.D. degree in physics from Tsinghua University, Beijing, China, in 2015.

He is currently a Lecturer with the College of Electronic and Information Engineering, Nanjing University of Aeronautics and Astronautics. His current research interests are in frequency-modulated continuous-wave (FMCW) detection and radio over free-space optics (RoFSO).

Jianing Zhao received the B.E. degree from the Nanjing University of Aeronautics and Astronautics, Nanjing, China, in 2019, where she is currently pursuing the Ph.D. degree with the Key Laboratory of Radar Imaging and Microwave Photonics, Ministry of Education. Her research interest is in microwave photonics measurement.

Fangzheng Zhang (Senior Member, IEEE) received the B.S. degree from the Huazhong University of Science and Technology (HUST), Wuhan, China, in 2008, and the Ph.D. degree from the Beijing University of Posts and Telecommunications (BUPT), Beijing, China, in 2013.

He is currently a Professor with the College of Electronic and Information Engineering, Nanjing University of Aeronautics and Astronautics. His current research interest includes microwave photonics and radar imaging.

Lejing Zhang is currently pursuing the bachelor's degree with the College of Electronic and Information Engineering, Nanjing University of Aeronautics and Astronautics, Nanjing, China.

Tianwen Yang is currently pursuing the bachelor's degree with the College of Electronic and Information Engineering, Nanjing University of Aeronautics and Astronautics, Nanjing, China.

Qinru Li is currently pursuing the bachelor's degree with the College of Electronic and Information Engineering, Nanjing University of Aeronautics and Astronautics, Nanjing, China.

Shilong Pan (Senior Member, IEEE) received the B.S. and Ph.D. degrees in electronic engineering from Tsinghua University, Beijing, China, in 2004 and 2008, respectively.

From 2008 to 2010, he was a Vision 2010 Postdoctoral Research Fellow with the Microwave Photonics Research Laboratory, University of Ottawa, Ottawa, ON, Canada. He joined the College of Electronic and Information Engineering, Nanjing University of Aeronautics and Astronautics, China, in 2010, where he is currently a Full Professor and an Executive Director of the Key Laboratory of Radar Imaging and Microwave Photonics, the Ministry of Education. His research has focused on microwave photonics, which includes optical generation and processing of microwave signals, analog photonic links, pho-tonic microwave measurement, and integrated microwave photonics. He has authored or coauthored more than 420 research articles, including more than 230 articles in peer-reviewed journals and 190 papers in conference proceedings.

Dr. Pan is a Fellow of OSA, SPIE, and IET. He is a Technical Committee Member of the IEEE MTT-3 Microwave Photonics and a Steering Committee Member of the IEEE International Topical Meeting on Microwave Photonics and the International Conference on Optical Communications and Networks. He has also served as the Chair of a number of international conferences, symposia, and workshops, including the TPC Chair of the International Conference on Optical Communications and Networks in 2015, and the TPC Co-Chair of the IEEE International Topical Meeting on Microwave Photonics in 2017. He is also an Associate Editor of *Electronics Letters* and a Topical Editor of *Chinese Optics Letters*. He was selected as an IEEE Photonics Society Distinguished Lecturer in 2019.